Available online at www.sciencedirect.com
SCIENCE DIRECT®
Icarus 167 (2004) 16–29
ICARUS
www.elsevier.com/locate/icarus

Deep Space 1 photometry of the nucleus of Comet 19P/Borrelly

B.J. Buratti,[a,*] M.D. Hicks,[a] L.A. Soderblom,[b] D. Britt,[c] J. Oberst,[d] and J.K. Hillier[e]

[a] *Jet Propulsion Laboratory, California Institute of Technology, 4800 Oak Grove Dr., Pasadena, CA 91009, USA*
[b] *United States Geological Survey, 2255 N. Gemini Dr., Flagstaff, AZ 86001, USA*
[c] *University of Tennessee, Department of Geological Sciences, Knoxville, TN 37996, USA*
[d] *Deutsches Zentrum für Luft-und Raumfahrt, Linder Höhe, 51147 Köln, Germany*
[e] *Department of Mathematics and Science, Grays Harbor College, Aberdeen, WA 98520, USA*

Received 24 September 2002; revised 29 April 2003

Abstract

The NASA-JPL Deep Space 1 Mission (DS1) encountered the short-period Jupiter-family Comet 19P/Borrelly on September 22, 2001, about 8 days after perihelion. DS1's payload contained a remote-sensing package called MICAS (Miniature Integrated Camera Spectrometer) that included a 1024 square CCD and a near IR spectrometer with ∼ 12 nm resolution. Prior to its closest approach of 2171 km, the remote-sensing package on the spacecraft obtained 25 CCD images of the comet and 45 near-IR spectra (L. Soderblom et al., 2002, Science 296, 1087–1091). These images provided the first close-up view of a comet's nucleus sufficiently unobscured to perform quantitative photometric studies. At closest approach, corresponding to a resolution of 47 meters per pixel, the intensity of the coma was less than 1% of that of the nucleus. An unprecedented range of high solar phase angles (52–89 degrees), viewing geometries that are in general attainable only when a comet is active, enabled the first quantitative and disk resolved modeling of surface photometric physical parameters, including the single particle phase function and macroscopic roughness. The disk-integrated geometric albedo of Borrelly's nucleus is 0.029 ± 0.006, comparable to the dark hemisphere of Iapetus, the lowest albedo C-type asteroids, and the uranian rings. The Bond albedo, 0.009 ± 0.002, is lower than that of any Solar System object measured. Such a low value may enhance the heating of the nucleus and sublimation of volatiles, which in turn causes the albedo to decrease even further. A map of normal reflectance of Borrelly shows variations far greater than those seen on asteroids. The two main terrain types, smooth and mottled, exhibit mean normal reflectances of 0.03 and 0.022. The physical photometric parameters of Borrelly's nucleus are typical of other small dark bodies, particularly asteroids, except preliminary modeling results indicate its regolith may be substantially fluffier. The nucleus exhibits significant variations in macroscopic roughness, with the oldest, darkest terrain being slightly smoother. This result suggests the infilling of low-lying areas with dust and particles that have not been able to leave the comet. The surface of the comet is backscattering, but there are significant variations in the single particle phase function. One region exhibits a flat particle phase function between solar phase angles of 50° and 75° (like cometary dust and unlike planetary surfaces), suggesting that its regolith is controlled by native dust rather than by meteoritic bombardment.

Keywords: Comets; Cometary nuclei; Deep Space 1; 19P/Borrelly

1. Introduction

As remnant bodies dating from the earliest stages of the Solar System, comets offer important clues to the processes involved in planet-building, and to the physical conditions in the primitive solar nebula. During their successive passages into the inner Solar System, comets undergo outgassing and possibly collisions with other objects. A glimpse at one of their nuclei thus offers a detailed view of the processes at work on their surfaces through time. The role comets could play in terrestrial mass extinctions and in the transport of volatiles and pre-biotic material to Earth renders an understanding of these processes particularly compelling. The reservoirs for comets are believed to exist within the vast reaches of the outer Solar System, in the Edgeworth–Kuiper belt and in the distant Oort cloud. One important set of questions centers on the relationships between asteroids, comets and Kuiper belt objects (KBOs). Some near Earth asteroids (NEAs) may be extinct cometary nuclei (Hicks, 1997; Fernandez et al., 2001; Weissman et al., 2003), while at least one asteroidal object, the Centaur 2060 Chiron (also

* Corresponding author.
E-mail address: bonnie.j.buratti@jpl.nasa.gov (B.J. Buratti).

0019-1035/$ – see front matter
doi:10.1016/j.icarus.2003.05.002

known as Comet 95P/Chiron), exhibits cometary activity. Telescopic views of cometary nuclei in the inner Solar System are precluded by the inevitable fate of a comet as it approaches the Sun: volatiles sublimate and drag surface dust to form a coma that obscures the bare nucleus. Much of the information about cometary nuclei has been obtained by photometric observations at aphelion, when the comet is least bright and most difficult to observe (Jewitt, 1991; Meech, 1991). These observations established that comets are small (1–20 km in diameter) and irregular, and gray or slightly red in color (Luu, 1993; Licandro et al., 2000; Lowry and Fitzsimmons, 2001). More recently, over 30 cometary nuclei have been characterized by Hubble Space Telescope CCD observations; in many cases careful subtraction of cometary coma has enabled analyses at smaller heliocentric distances (Lamy et al., 2003). Thermal measurements established low geometric albedos (0.02 to 0.07) for a number of comets, including Arend–Rigaux, Neujmin 1, and Tempel 2 (Veeder et al., 1987; Campins et al., 1987; Tokunaga et al., 1992). Radar observations establish surface roughness on meter-scales (Harmon et al., 1989; Campbell et al., 1989). Rotational periods of comets range from a few hours to several days, and they tend to be slightly longer than those of asteroids (De Pater and Lissauer, 2001). The spin state often involves complex rotation around non-principal axes, due to the outgassing of volatiles and consequent torques that alter the angular momentum vector (Belton, 1991). Due to the small size of cometary nuclei and the inherent difficulties in observing them, a spacecraft encounter represents an unprecedented opportunity to scrutinize and understand them. The first close view of a cometary nucleus was obtained by the Vega 1, Vega 2, and Giotto spacecraft in 1986 during their flybys of Comet P/Halley. Although obscuration of the nucleus by a dusty coma precluded quantitative, disk resolved photometry, some basic physical information on its nucleus was obtained, including a size of about 16 by 8 km (Keller, 1990), and an albedo of 0.04 ± 0.02 (Sagdeev et al., 1986). Telescopic observations of Halley combined with the spacecraft-derived size yielded a visual geometric albedo of $0.05^{+0.03}_{-0.01}$ (Hughes, 1985).

The NASA-JPL Deep Space 1 Mission (DS1), the first interplanetary mission to be propelled by an ion-propulsion drive, encountered the short-period Jupiter-family Comet 19P/Borrelly on September 22, 2001, about 8 days after perihelion. Borrelly is the archetype and eponym of the second-most common class of comets, the Borrelly group, which are depleted in carbon-chain molecules (A'Hearn et al., 1995) yet similar in water and ammonia ratios relative to the more common Halley group of comets (Fink et al., 1995). The primary physical properties of Borrelly are summarized in Table 1. During the comet's rotational period of 25 ± 0.5 hours, it exhibits an amplitude of 0.95 magnitudes (Lamy et al., 1998), consistent with a principal axis ratio of 0.41, if one assumes that the change in brightness is due to shape alone and that the lightcurve was obtained when the axis of rotation was perpendicular to the line of sight. This ratio is consistent with the values of 4.0 ± 0.1 and 1.58 ± 0.06 km for the principal axes determined by the highest resolution image returned by DS1 (Fig. 1). The dust production during the encounter was several factors of 10 below that of the Halley encounter, permitting a nearly clear view of the nucleus (Soderblom et al., 2002). Images show a fan-shaped jet emitted from a discrete active area on the sunward side of the comet, and at least two collimated jets. DS1's payload contained a remote-sensing package called MICAS (Miniature Integrated Camera Spectrometer) that included a 1024 square CCD, a near IR spectrometer with ~ 12 nm resolution, an Active Pixel Sensor Camera, and a UV spectrometer. Prior to the closest approach of 2171 km, the remote-sensing package on the spacecraft obtained 25 CCD images of the comet and 45 near IR spectra. The main results of the flyby, the behavior of MICAS, and the IR spectra have been de-

Table 1
Borrelly: major characteristics

Albedo	0.029 ± 0.006[a]
Principal axes (km)	$4.0 \pm 0.1 \times 1.58 \pm 0.06$[a]
Rotational period	25 ± 0.5 hours[b]
Period	7 years[c]
Perihelion	1.36 AU[c]
Orbital inclination	30°[c]
Orbital eccentricity	0.62[c]
Discovery	Alphonse Borrelly (France), 1904
OH production	2×10^{28} molecules/s[d]

[a] This study.
[b] Lamy et al. (1998).
[c] JPL Horizons database (www.horizons.jpl.nasa.gov).
[d] A'Hearn et al. (1995).

Fig. 1. The closest image (Near_1) obtained by the MICAS CCD camera on September 22 2001 at 22:26:43 UT. The distance to the surface is 3556 km, the resolution is 47 m/pixel, and the solar phase angle is 52°.

scribed elsewhere (Soderblom et al., 2002). The maximum spatial resolution attained was 47 meters per pixel.

In this paper we describe the results of the first quantitative, disk resolved photometric study of a comet's nucleus. Our results include the derivation of fundamental photometric quantities such as the geometric and Bond albedos, the solar phase curve and phase integral; the derivation of disk-integrated physical photometric parameters such as the single scattering albedo, the single particle phase function, and macroscopic roughness; and disk resolved roughness and particle phase functions. Finally, we construct a map of normal reflectances on the comet's surface to study how the range and distribution of these albedos relates to the comet's geologic features and evolution.

2. Observations

During the 90-minutes before closest approach, the MICAS CCD camera acquired 25 images spanning a range in solar phase angles of 88° to 52°. The images are listed in Table 2, along with relevant timing and geometric information. These images are the first resolved views of a cometary nucleus entirely unobscured by dust, as well as the first measurements of the surface of a cometary nucleus at large phase angles. When the nucleus of a comet is visible at aphelion, it is possible to observe it only over a restricted range of small solar phase angles. For example, the maximum excursion in phase angle at 3 AU is 18°. Since large phase angles are necessary to accurately determine both the roughness of a surface and the single particle phase function (Helfenstein et al., 1988; Buratti, 1991), these observations enable the first determination of these physical photometric parameters of a comet's surface.

The images were obtained with a frame transfer CCD detector consisting of an array of 1024 × 1024 pixels, each having a field-of-view of 9 μrad. The CCD camera carried no filter system; it exhibited a broadband response in the 500 to 1000 nm range with an effective wavelength of 660 nm. Integration times ranged from 1.75 to 0.077 seconds. The images were radiometrically and geometrically calibrated using procedures and files developed at JPL and USGS Flagstaff. Preflight bench calibrations at JPL included measurements of geometric distortions on the image field, the flatfield and radiometric response of the CCD. During cruise, the radiometric calibrations were affirmed by observing standard targets including Mars, Jupiter, and α-Bootes (Arcturus). Preliminary results on Borrelly's geology, its shape, the morphology of its jets, and its photometry have been discussed in Soderblom et al. (2002). The best resolution image, obtained at a distance of 3556 km from the comet's surface, is shown in Fig. 1. Figure 2 is an image of 19P/Borrelly obtained with the Large Format Camera at the 200-inch Hale telescope on 16 September 13:00 UT, approximately one week prior to Deep Space 1's encounter.

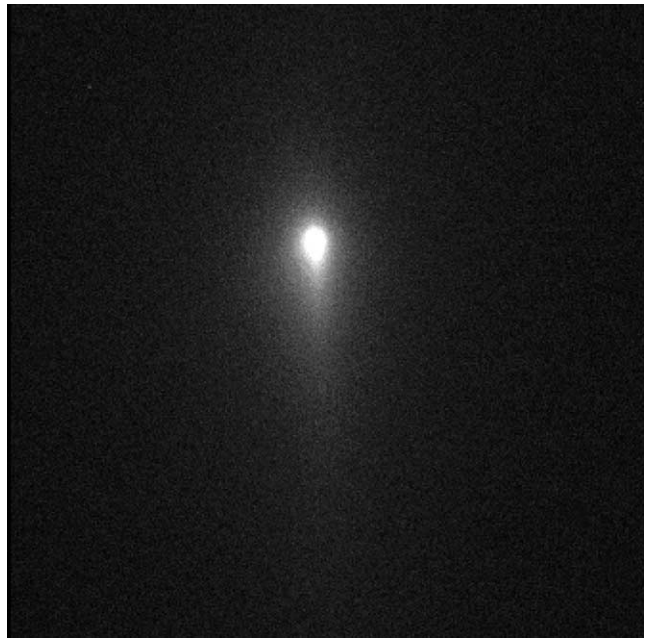

Fig. 2. An image of 19P/Borrelly obtained with the 200-inch Hale telescope on Palomar Mountain and the Large Format Camera (R-filter) on 16 September 2001 13:00 UT. The solar phase angle is 41° and the heliocentric distance is 1.36 AU. The image is approximately 100,000 km square.

Absolute radiometric calibrations of the camera appear to be good to at least the 10–15% level. Extrapolation of the average surface I/F given in Soderblom et al. (2002) to 0° degrees results in a geometric albedo of 0.024. (I is the specific intensity and πF is the incident solar flux.) Accounting for an opposition surge of 0.25 magnitudes, typical of a C-type asteroid (Helfenstein and Veverka, 1989), yields a geometric albedo of 0.03, in good agreement with that derived in Section 3 from HST (Lamy et al., 1998) and ground-based photometry (Rauer et al., 1999) and the DS1-determined size.

3. Disk-integrated photometry

Disk integrated photometric measurements as a function of solar phase angle yield some of the fundamental parameters of a planetary surface: the geometric albedo, the phase integral, and the Bond albedo, a necessary parameter for thermal modeling. A disk integrated phase curve was derived for Borrelly by integrating the DNs in each pixel of the images listed in Table 2, and then scaling the derived brightness to a common spacecraft distance. Coma was subtracted from each image by estimating its intensity from the ambient dark sky. Typically the intensity of the coma was only 1–2% of the intensity of the surface; on the final image it was much less than 1%. The results are shown in Fig. 3, together with ground based and HST observations of Borrelly's nucleus at smaller solar phase angles of 3° to 38° (Lamy et al., 1998; Rauer et al., 1999; Weissman et al., 1999). The ground-based observations have been corrected to the maximum of Bor-

Table 2
Images used in this study

Expos.	Image file name	Image UTC	Range (km)	α	Sun–spacecraft–comet angle
0.154	snip21_06_51.pds	21:05:47	83380	87.6	92.4
0.874	CCD_far_1_4.pds	21:06:17	82882	87.6	92.4
1.750	CCD_far_1_5.pds	21:06:47	82385	87.6	92.4
0.307	snip22_00_11.pds	21:59:07	30358	85.0	95.0
0.307	snip22_01_11.pds	22:00:07	29366	84.9	95.1
0.307	snip22_02_11.pds	22:01:07	28374	84.7	95.2
0.307	snip22_03_11.pds	22:02:07	27382	84.6	95.4
0.307	snip22_04_11.pds	22:03:07	26390	84.4	95.6
0.307	snip22_05_11.pds	22:04:07	25398	84.2	95.8
0.307	snip22_06_11.pds	22:05:07	24407	84.0	96.0
0.307	snip22_07_11.pds	22:06:07	23416	83.8	96.2
0.307	snip22_08_11.pds	22:07:07	22425	83.6	96.4
0.307	snip22_12_36.pds	22:11:32	18056	82.3	97.7
0.307	snip22_13_36.pds	22:12:32	17069	81.9	98.2
0.307	snip22_14_36.pds	22:13:32	16082	81.4	98.6
0.307	snip22_15_36.pds	22:14:32	15097	80.9	99.1
0.307	snip22_16_29.pds	22:15:25	14228	80.4	99.6
0.154	snip22_17_06.pds	22:16:02	13621	79.8	100.0
0.109	CCD_mid_1_2.pds	22:20:25	9341	75.5	104.3
0.109	CCD_mid_2_2.pds	22:21:30	8297	73.8	106.0
0.109	CCD_mid_4_1.pds	22:23:16	6616	69.9	110.0
0.077	CCD_mid_5_3.pds	22:25:43	4387	59.6	120.4
0.077	CCD_near_1.pds	22:26:43	3556	51.6	128.4

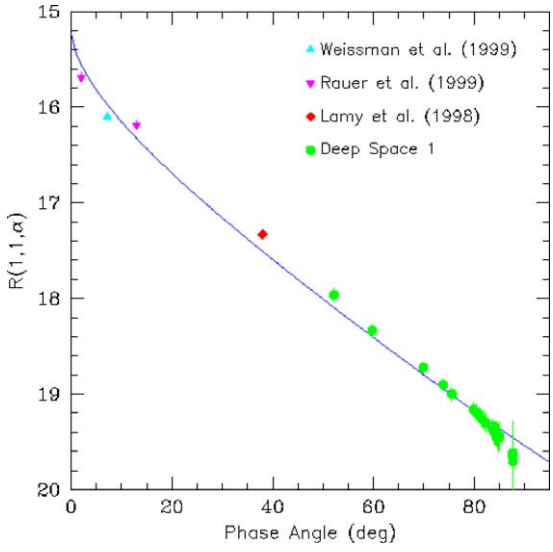

Fig. 3. The disk-integrated phase curve of Borrelly constructed from MICAS images and HST and ground-based observations with the global physical model summarized in Table 4. The MICAS measurements, with an effective wavelength of 0.660 μm have been merged with ground-based R-filter data.

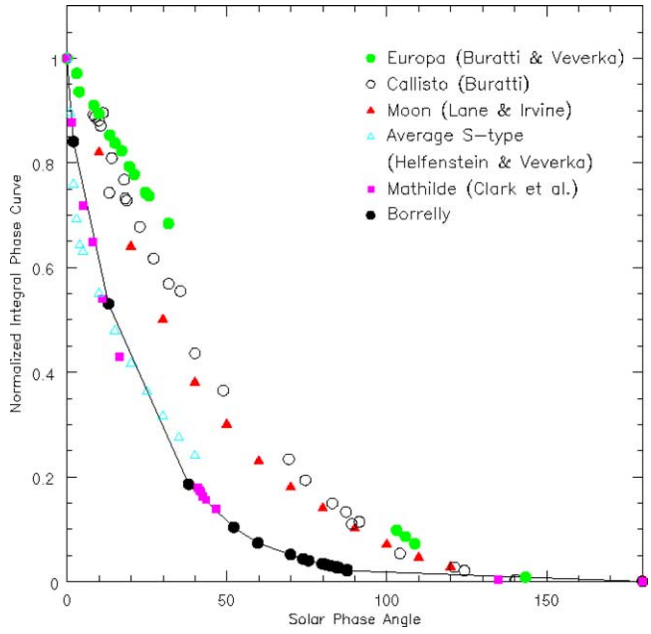

Fig. 4. The phase curves of other airless bodies in the Solar System, normalized to unity at zero degrees. The phase curve of Borrelly is most similar to those of other low-albedo bodies, particularly the C-type asteroid 253 Mathilde. The observations are from Buratti and Veverka (1983), Buratti (1991), Lane and Irvine (1973), Helfenstein and Veverka (1989), and Clark et al. (1999).

relly's lightcurve, since the spacecraft encounter occurred during that rotational phase.

Figure 4 shows Borrelly's solar phase curve with examples of other Solar System objects (the curves are normalized to unity at 0°). Borrelly's derived phase curve is very similar to that of the C-type asteroid 253 Mathilde, which was investigated by the NEAR spacecraft in 1997 (Veverka et al., 1997; Clark et al., 1999), and to a composite S-type asteroidal phase curve out to ∼ 40 degrees derived by Helfenstein and Veverka (1989). A measurement of the phase function of Comet 28P/Neujmin 1 showed it to be less steep than the typical phase curve of C-type asteroids (Delahodde et al., 2001).

Table 3
Geometric and Bond albedos of Borrelly and other small low-albedo bodies

Object	p_v*	q	A_B	Source
Borrelly	0.029 ± 0.006	0.28 ± 0.03	0.009 ± 0.002	This study
Halley	$0.04 + 0.01/-0.02$			Sagdeev et al. (1986)
Mathilde	0.047 ± 0.005	0.28 ± 0.035	0.013 ± 0.003	Clark et al. (1999)
Deimos	0.068	0.39	0.027	Thomas et al. (1996)
Phobos	0.071	0.30	0.021	Simonelli et al. (1998)
C-type	0.02–0.09			Tedesco et al. (1989)
D-type	0.029–0.05			Tedesco et al. (1989)
Iapetus	0.01–0.10			Buratti and Mosher (1995)
(low albedo hemisphere)				
Uranian rings	0.032 ± 0.003			Ockert et al. (1987)

* The derived albedo for Borrelly was obtained at the effective wavelength of the MICAS camera, 660 nm.

The geometric albedo of Borrelly can be obtained directly from the measurements in Fig. 3 and the DS1—determined size. Extrapolating to a phase angle of zero degrees with a Mathilde-like phase curve below 3 degrees, and correcting to the mean of the lightcurve to obtain an opposition magnitude of 15.97, we find that the geometric albedo is 0.029 ± 0.006 at 660 nm. This value is lower than that of 0.04 assumed by Lamy et al. (1998). The error bars on Lamy et al.'s size (4.4 ± 0.3 for the major principal semiaxis, and 1.8 ± 0.18 for the minor principal semiaxis) translate into a 35% uncertainty in the geometric albedo. When given our own error bars of 21% for the geometric albedo, due also primarily to errors in Borrelly's effective projected area, the DS1 and HST results are seen to be fully consistent.

The phase integral, which describes the directional scattering properties of a planetary surface, is given by (Horak, 1950):

$$q = 2 \int_0^{\pi} \Phi(\alpha) \sin\alpha \, d\alpha, \tag{1}$$

where $\Phi(\alpha)$ is the normalized disk-integrated brightness (Fig. 4). The observations of Borrelly by DS1 at large solar phase angles enable the first measurement of the phase integral and Bond albedo of a comet. A four-point Gaussian quadrature of Borrelly's phase curve (Chandrasekhar, 1960) yields a phase integral of 0.27 ± 0.01. The Bond albedo, a value which expresses the fraction of energy reflected from the surface to that received from the Sun, is given by $A_B = p \cdot q$. The Bond albedo is a fundamental parameter for understanding the energy transport, equilibrium temperatures, and vapor pressures for various surface volatiles. Borrelly's Bond albedo is 0.009 ± 0.002, the lowest of any object in the Solar System so far measured. Table 3 lists the geometric and Bond albedos and the phase integral of Borrelly and other small low-albedo bodies for comparison. Between 10 and 30 degrees, the phase coefficient of Borrelly is 0.024 ± 0.002 magnitudes per degree, comparable to the values for 243 Ida (0.027 mags/deg) and 951 Gaspra (0.025 mags/deg), but smaller than that of 253 Mathilde (0.040) (Clark et al., 1999).

The geometric albedo of Borrelly is low, but comparable to that of other objects (or specific areas of objects) located primarily in the outer Solar System, including the lowest albedo C-type (carbonaceous chondritic) asteroids, the dark side of Iapetus, the uranian rings (Ockert et al., 1987), and other comets. At least 10 C-type asteroids have visual geometric albedos of 0.030 or less, with minimum albedos of 0.02 (Tedesco et al., 1989). The dark hemisphere of Iapetus has normal reflectances as low as 0.01 or lower (Buratti and Mosher, 1995). Other cometary nuclei have albedos in the 0.02 to 0.03 range (Campins et al., 1987; Veeder et al., 1987), including possibly Halley with an albedo of 0.04 ± 0.02 (Sagdeev et al., 1986). Finally, several asteroids in comet-like orbits have albedos between 0.019 and 0.038, if one assumes a slow-rotator thermal model (Fernandez et al., 2001).

4. A map of normal reflectance

A map expressing the intrinsic reflectivity of a planet or small body is an important tool for understanding geophysical relationships on its surface. Albedo maps of other objects provided decisive clue as to the mechanisms for surface alterations. For example, the albedo map of Iapetus offered key evidence for an exogenous origin to its dark surface (Squyres et al., 1984; Buratti and Mosher, 1995). Because a comet is a dynamic, changing body, an albedo map is especially valuable for understanding the evolution of its surface. Coupled with physical information on the roughness and microtexture of the surface (Section 5) an albedo map represents a powerful tool for answering important questions such as: How large are the variegations in albedo on the comet's surface? Are the comet's active regions connected to a specific surface reflectivity? Is there evidence for past activity? If so, how much of the surface has been active in the past? Is there evidence for exogenously produced changes on the surface, caused by such processes as meteor or solar wind bombardment? How does the albedo of the comet change with time?

Much (often most) of the variations in I/F on a spacecraft image are not intrinsic; rather they are caused by changes in the local surface normal vector with corresponding changes in the radiant incident and emission angle. (Here I is the intensity of scattered sunlight and πF is the incident solar flux.) If the image is not obtained at zero solar phase angle, there is the additional effect of the solar phase function, which contains physical information on the surface, such as its macroscopic roughness, the size and size-distribution of particles in the optically active upper layer of the regolith, and the packing state of those particles (Section 5). Modeling the changing radiance incident and emission angles on a comet is particularly challenging because of its nonspherical shape. Although the mathematics of a triaxial ellipsoid have been worked out (Noland, 1975), comets cannot in general be approximated by that simple a shape.

Here we employ a shape model in which the limb and terminator are used as continual constraints. The model fits semicircular arcs of a pixel's width between the limb and terminator along the Sun line. The emission and incident angles for each pixel are then determined from the resulting surface normal. To correct the I/F in each individual pixel to a normal reflectance (for which all three of the incident, emission, and solar phase angles are 0°), we use the Lommel–Seeliger photometric function (see Section 5) for which the normal reflectance can be derived from (Veverka, 1970):

$$I(\mu, \mu_0, \alpha)/F = f(\alpha) r_n \mu_0 / \pi(\mu + \mu_0), \tag{2}$$

where r_n is the normal reflectance, μ and μ_0 are the cosines of the emission and incident angles, respectively, and $f(\alpha)$ is the solar phase function. The function $f(\alpha)$ contains important physical information about the surface, which will be derived in Section 5.

The highest resolution image, which is also the image obtained at the minimum phase angle (Table 2) was used to derive a map of normal reflectances. For a Lommel–Seeliger photometric function, the normal reflectance is equivalent to the geometric albedo. The function $f(\alpha)$ was determined by constraining the average of the resulting normal reflectances to be equal to the geometric albedo determined in Section 3. Figure 5 shows the resulting map in both continuous (top) and contour (bottom) formats. Figure 6 is a scan of normal reflectances extracted from a line traversing the length of Borrelly. Figure 7 is a histogram showing the range in normal reflectances on the surface of the comet's nucleus.

Borrelly exhibits large albedo variegations on its surface, far more than are typical of other minor bodies. About 95% of the albedos fall between 0.02 and 0.04, a range of a factor of two, with variations of a factor of three between the highest albedo and lowest albedo regions of the surface. In contrast, approximately 95% of the surface normal albedos on 253 Mathilde fall between 0.04 and 0.057 (Clark et al.,

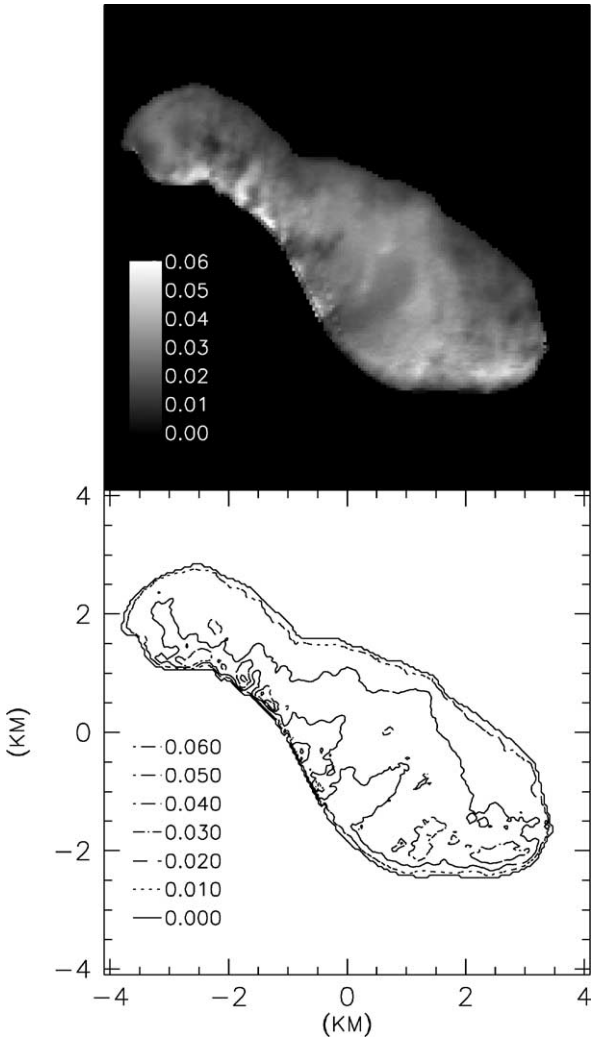

Fig. 5. A map of Borrelly's normal reflectance. A Lommel–Seeliger (lunar) photometric model and the phase curve illustrated in Fig. 3 were adopted to perform photometric corrections.

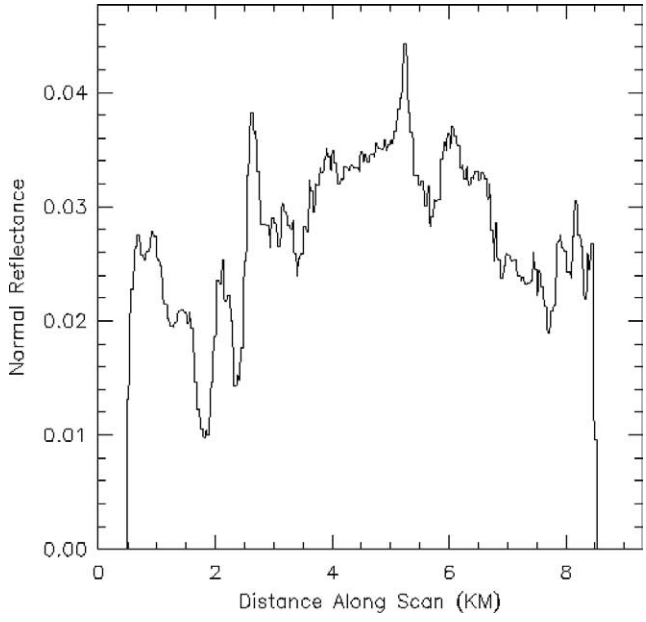

Fig. 6. A scan of normal reflectance extracted from the map in Fig. 5 along the largest dimension of Borrelly.

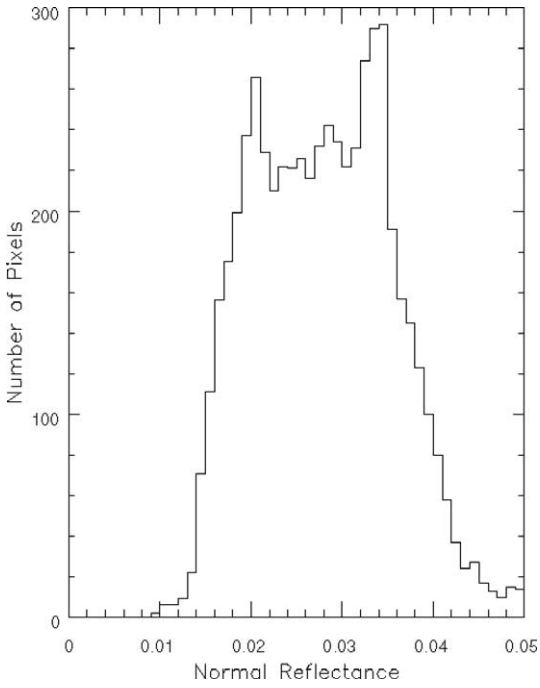

Fig. 7. A histogram of normal reflectance derived from the map in Fig. 5.

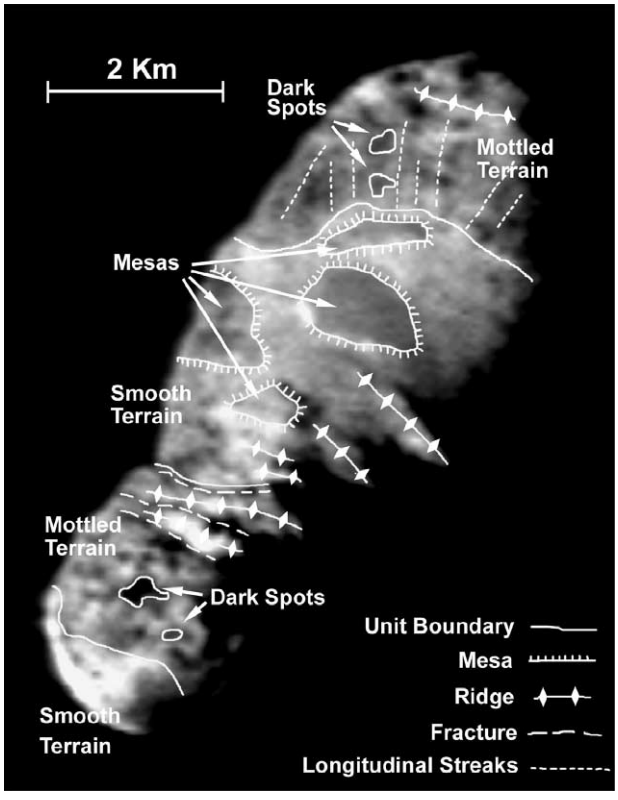

Fig. 8. A geologic map of Borrelly (Britt et al., 2002).

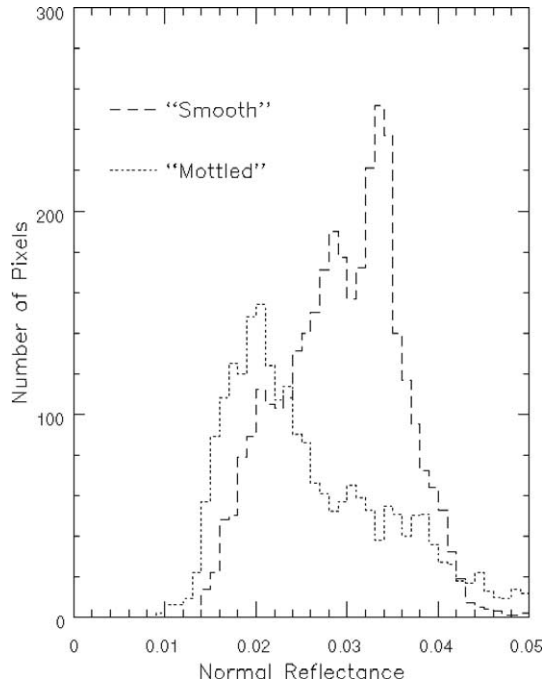

Fig. 9. Histograms of normal reflectances for the two major terrain types depicted in Fig. 8: mottled and smooth terrains.

1999), while on Phobos, the small, C-type (probably captured) satellite of Mars, ∼ 95% fall between 0.06 and 0.09. S-type asteroids exhibit a similarly constrained range: the 95% metric on 951 Gaspra is ∼ 0.18 to ∼ 0.26 (Helfenstein et al., 1994); while on 243 Ida it is ∼ 0.19 to 0.25, with a slight bifurcation between two terrains (Helfenstein et al., 1996). The variegations exhibited by Borrelly are more typical of the surfaces of small bodies with recent active geologic processes or significant surficial alteration mechanisms. For example, albedo variegations of up to a factor of two appear on the saturnian satellites (Buratti, 1985).

Is there a difference in albedo and albedo-range among the various terrains mapped on the comet? Figure 8 is a geologic map produced from the Near_1 image (Britt et al., 2002; Soderblom et al., 2002). Histograms for the two primary terrain units ("mottled" and "smooth" terrain) are shown in Fig. 9. There is a significant difference in albedo between the two terrains: The mean normal reflectance of the smooth terrain is ∼ 0.03, while the corresponding value for the mottled terrain is ∼ 0.022. However, substantial inhomogeneities and overlap in albedos exist between the two terrains, a fact which is also evident from the albedo map (Fig. 5).

5. Physical photometric properties

Physical photometric models express the radiation reflected from a planetary surface in terms of the following physical parameters: the single scattering albedo (w); the single particle phase function, $P(\alpha)$; a function describing the opposition effect, $S(\alpha)$, which depends primarily on the compaction state of the surface and the particles' sizes and size distribution; and a function describing the macroscopic roughness of the surface, $M(\mu, \mu_0, \alpha)$. For a surface in which multiple scattering is insignificant

(which is certainly true of Borrelly; see Veverka et al., 1978; Buratti, 1985), the specific reflected intensity is given by (Chandrasekhar, 1960):

$$I(\mu, \mu_0, \alpha)/F = f(\alpha) w \mu_0 / 4(\mu + \mu_0), \quad (3)$$

where

$$f(\alpha) = P(\alpha) S(\alpha) M(\mu, \mu_0, \alpha). \quad (4)$$

The function $f(\alpha)$ is the surface solar phase function, which contains physical information about the surface. Observations at small solar phase angles (0° to ∼ 12°) are particularly important for understanding the compaction state of the optically active portion of the regolith: this is the region of the well-known opposition effect, in which the rapid disappearance of shadowing among particles causes a nonlinear surge in brightness as the object becomes fully illuminated. Less compacted, fluffy regoliths tend to have more pronounced surges, if all other factors, such as albedo, are equal. In addition, the coherent backscatter of radiation can contribute to the surge, particularly for high albedo objects (Hapke, 1990). One widely used model that characterizes the shadow-hiding mechanism in planetary surfaces is that of Hapke (1986). The model characterizes the opposition surge in terms of the amplitude of the surge (B_0), and the width of the surge, which in turn is related to the compaction parameter h. A higher h corresponds to a more compacted surface with less space between particles.

Macroscopically rough features, ranging in size from clumps of several particles to mountains, craters, and ridges, cast shadows and alter the local incidence and emission angles. Two models describing surficial roughness have been developed: In one the surface is covered by a specified fraction of paraboloidal craters characterized by their depth-to-diameter ratio (Buratti and Veverka, 1985); in the other, the surface is covered by features defined by a mean slope model (Hapke, 1984). Even though Borrelly appears to be devoid of craters (Soderblom et al., 2002) the idealized crater shape can represent concavities on its surface. The derivation of macroscopic roughness offers clues to the impact and outgassing history of cometary nuclei. Comparison of a roughness model of a cometary nucleus with similar models of asteroids and other minor bodies will help to establish evolutionary relationships and similarities among them. Regional differences in roughness on a cometary nucleus provide an empirical basis for the evolutionary path of a comet, including evidence of past activity in specific regions. Finally, roughness models enable the description of rough features *below the resolution limit of the camera*, because the models are scale-invariant.

The single particle phase function is an indicator of the physical character of the individual particles in the upper regolith, including their size distribution, shape, and optical constants. It can be simply expressed by an empirical expression that was derived to describe dust in the interstellar medium (Henyey and Greenstein, 1941):

$$P(\cos\theta, g) = \left(1 - g^2\right) / \left(1 + g^2 - 2g\cos\theta\right)^{3/2}, \quad (5)$$

where the scattering angle $\theta = (180° - \alpha)$ and g is the asymmetry factor describing the directional scattering properties of individual particles. A g of -1 corresponds to pure backscattering, $+1$ corresponds to pure forward scattering, and 0 describes isotropic scattering. Small or transparent particles tend to be more isotropically scattering because photons survive to be multiply scattered; forward scattering can exist if photons exit in the direction away from the observer. For cometary nuclei, knowledge of the mean particle size is important for understanding the degree to which the surface has been subjected to such process as comminution of particles by meteoritic impacts and annealing mechanisms. Do comets even have regoliths? Another important question concerns the degree of physical similarity between cometary dust and the particles comprising the surface.

The unique derivation of physical parameters requires the acquisition of measurements at certain critical solar phase angles (Helfenstein and Veverka, 1989). To characterize the opposition surge, observations at solar phase angles less than 12° (ideally less than 6°) are required. Observations at large phase angles (> 50°) are required to characterize roughness (although careful analysis of limb darkening at smaller phase angles is also an effective means to understand roughness; see Buratti and Veverka, 1985). Finally, the determination of the single particle phase function needs measurements at both large and small phase angles. DS1 observations coupled with ground-based measurements at small phase angles offer a range in viewing geometries to derive the first physical photometric parameters for a comet's nucleus. In particular, the observations at large solar phase angles are key to understanding the degree of macroscopic roughness: such observations are not possible from Earth because comets become active at the small heliocentric distances required for large solar phase angles.

Physical photometric models have been fit to a wide variety of objects, including the asteroids 951 Gaspra (Helfenstein et al., 1994), 243 Ida (Helfenstein et al., 1996), and 253 Mathilde (Clark et al., 1999). One criticism of photometric models is that they are limited by the physically idealized assumptions that go into them. But with the large number of planetary bodies that have been studied, *comparisons* among objects are valuable in understanding their comparative properties and their interrelationships.

5.1. Global photometric parameters

The measurements in Fig. 3 can be fit to Eq. (3) to derive global photometric parameters for Comet Borrelly. Using a model that fits a mean slope angle (θ), single scattering albedo (w), and asymmetry parameter (g), and the opposition surge amplitude and width, we find the values listed in Table 4, along with the equivalent parameters of other small bodies for comparison. The compaction state of Borrelly's regolith is lower than that of other small bodies, although we note that with only a single (ground-based) data point in the region of the opposition surge, we do not consider this

Table 4
Physical photometric parameters of selected small bodies

Object	w	g	Mean slope angle (°)[a]	h	B_0	Source
Borrelly	0.020 ± 0.004	-0.45 ± 0.05	20 ± 5	0.0084 ± 0.005	1.0 ± 0.5	This study
253 Mathilde	0.035 ± 0.006	-0.25 ± 0.04	19 ± 5	0.074 ± 0.003	3.18 ± 1.0	Clark et al. (1999)
Deimos	0.079	−0.29	16.4	0.068	1.65	Thomas et al. (1996)
Phobos	0.054	−0.13	21			Simonelli et al. (1998)
243 Ida	0.22	−0.33	18	0.02	1.53	Helfenstein et al. (1996)
951 Gaspra	0.36	−0.18	29	0.06	1.63	Helfenstein et al. (1994)
C-type	0.037	−0.47	20	0.025	1.03	Helfenstein and Veverka (1989)
S-type	0.23	−0.27	20	0.08	1.60	Helfenstein and Veverka (1989)
Moon	0.25	−0.25	20	0.05 ± 0.01	1.0 ± 0.1	Buratti (1985), Hillier et al. (1999)

[a] The best-fit depth-to-diameter ratio for the crater roughness model, which was fit only to the Borrelly data, is 0.32.

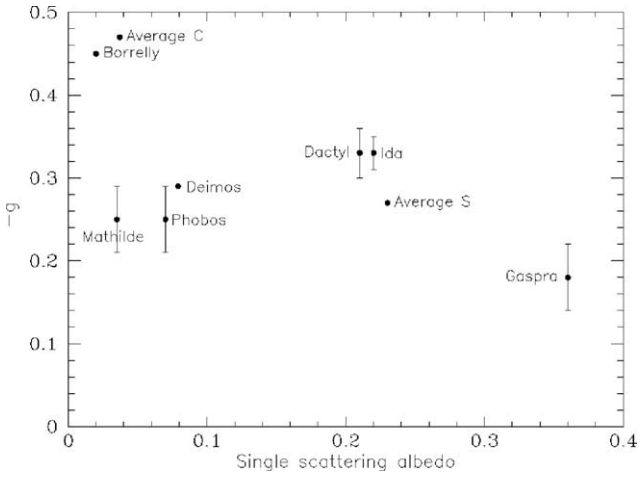

Fig. 10. The Henyey–Greenstein asymmetry parameter (g) as a function of single scattering albedo (w) for small bodies. Borrelly exhibits the most similarity for these parameters to C-type asteroids.

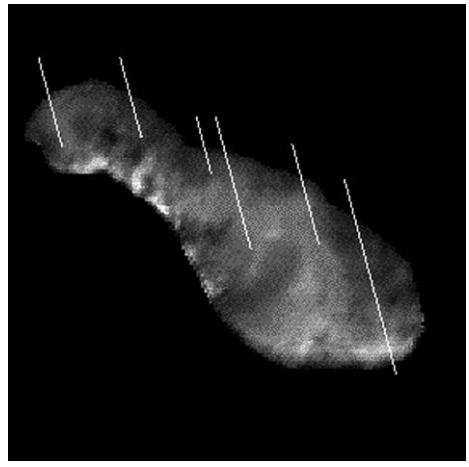

Fig. 11. The location of scans of I/F which were extracted from Near_1 for fits to roughness models. From right to left, the lines are one through six.

result solid. Borrelly shares the strong backscattered phase function of C-type asteroids (Fig. 10) and it is even more backscattering than Mathilde.

5.2. Disk resolved photometric properties

Although disk-resolved images at moderate spatial resolution (> 100 m) exist only between solar phase angles of 52° and 70°, some disk-resolved information on the macroscopic roughness and on the single particle phase function can be derived. The effects of macroscopic roughness become pronounced at these phase angles, and the functional form of a surface scan of the reflected intensity vs. the photometric longitude depends sensitively on the slope angle or depth-to-diameter ratio of rough facets (Hapke, 1984; Buratti and Veverka, 1985). For the crater-roughness model, the position of an inflection in the scan is a function of the depth-to-diameter ratio of asperities on the surface. Figure 11 shows the positions of six scans of I/F extracted from the nucleus of Borrelly; two of the scans are in mottled terrain, and four of the scans are in "smooth" terrain (see Fig. 8). A best-fit crater-roughness solution for each of these scans is shown in Fig. 12 and summarized in Table 5, with an equivalent Hapke roughness parameter for comparison. Disk-resolved differences in roughness clearly exist on the surface of Borrelly, with "smooth" terrain actually tending to be somewhat rougher (although the "smoothest" scan is at the narrow point of the nucleus, in smooth terrain). The base of Borrelly's jets tend to be low-albedo regions located in the mottled terrain (Soderblom et al., 2002). This observation is consistent with comet's surface becoming progressively darker as brighter volatile material is outgassed. The "smooth" terrain which is higher in albedo and more uniform in albedo may thus be relatively unaltered terrain. It may also be uniform due to cometary dust that fell back onto the nucleus. Our results suggest that the effect of outgassing is to make the surface of the comet smoother, as well as darker, as lag deposits are left behind. The narrowest part of Borrelly may also be the most outgassed, as it is the smoothest.

Disk resolved information on the single particle phase function can also be derived from the images at high and medium resolution. The surface solar phase function, $f(\alpha)$, which contains information about the physical nature of the surface, can be approximated at phase angles of 50°–70° by:

$$f(\alpha) = P(\alpha)M(\alpha). \tag{6}$$

Figure 13 gives the $f(\alpha)$ derived from Eq. (3) for three regions of the comet that could be followed through the full

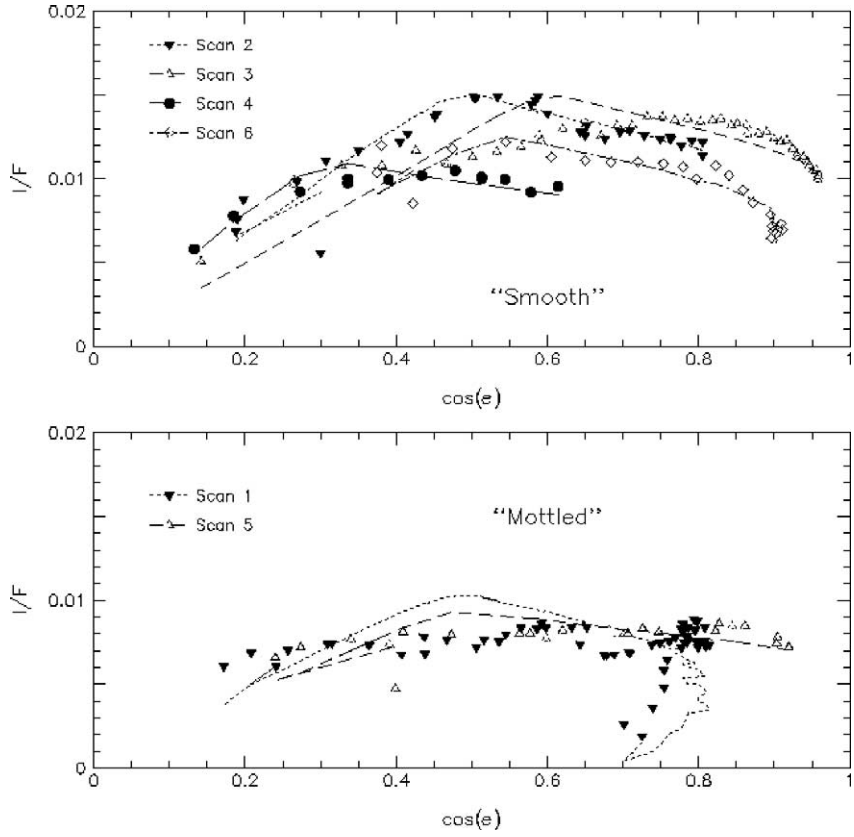

Fig. 12. The scans from the two terrains (Fig. 11), fit to roughness models summarized in Table 5. Except for one scan, the "smooth" terrain is slightly rougher (although this difference is not significant within the goodness of the fit to the models.)

Table 5
Regional roughness solutions

Line	Terrain	Q, depth to diameter (± 0.04)	θ, mean slope angle (°) (± 3 degrees)
1	Mottled	0.29	20
2	Smooth	0.29	20
3	Smooth	0.39	25
4	Smooth	0.17	13
5	Mottled	0.29	20
6	Smooth	0.34	23

Lines are read right to left from Fig. 11.

Table 6
Regional roughness and single particle phase functions

Region	Depth to diameter (Q)	Mean slope angle (θ, degrees)	Asymmetry parameter (g)
Central bright	0.39 ± 0.08	25 ± 5	-0.25 ± 0.03
Small end bright	0.34 ± 0.07	23 ± 5	-0.38 ± 0.05
Small end dark spot	0.3 ± 0.1	20 ± 7	0.05 ± 0.03

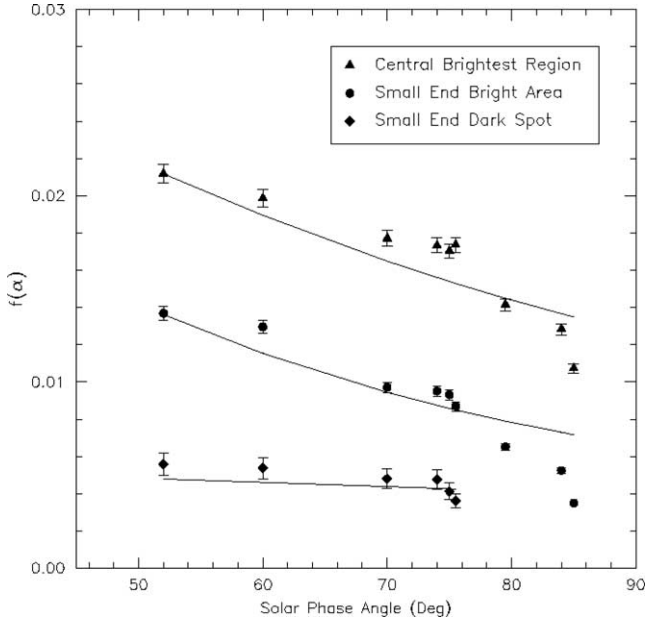

Fig. 13. A model of best-fit $f(\alpha)$ and roughness for various regions observed through a range of solar phase angles. The fits are summarized in Table 6. The particle phase function for the dark spot is nearly isotropic, which is not characteristic of other planetary surfaces.

range of solar phase angles: the central bright region, a bright region on the small end, and a dark region on the small end. These curves were fit to the crater roughness model and a single parameter Henyey–Greenstein single particle phase function to yield the values listed in Table 6 (the equivalent Hapke mean slope parameter is listed for comparison). Although differences in roughness are modest, we find substantial differences in the particle phase function between these various terrains, a result that indicates there are variations in particle size, shape, and composition on the comet's surface.

The highest albedo region of the comet contains the particles that backscatter less than the comet as a whole, indicating small particles that are transparent to visible photons, such as grains of ice. Although no water ice was observed on the surface of the comet (Soderblom et al., 2002), the photometric properties provide evidence for it. This result also affirms the view that the high albedo "smooth" terrain is the least outgassed region of the comet. An alternate explanation is that the greater degree of multiple scattering in the higher albedo region "isotropizes" the reflected light, as multiply scattered photons tend to be reflected in random directions. We find this explanation unlikely, as "high" albedos on the comet's surface are still too low for multiple scattering to be at all significant (Veverka et al., 1978). However, the most isotropically scattering segment of the surface is that of the small dark spot. This region is similar to those forming the base of active jets (Soderblom et al., 2002), and it is very likely an outgassed region of the comet. Its phase function, which is isotropic to within the errors of our model fit, is very similar to that of the coma (Soderblom et al., 2002). Since the visual phase function of the coma is due to cometary dust, our results imply that the dark spots may consist of a lag deposit of a material that is similar to the dust in the coma, or even of dust that has fallen back onto the surface.

6. Summary, discussion, and future work

The Deep Space 1 flyby of Comet 19P/Borrelly provided the first close-up view of a cometary nucleus unobscured by its coma. The images provided an opportunity to perform the first disk-resolved photometric studies of a comet. The images were obtained at large solar phase angles ideal for understanding macroscopic roughness and the phase functions of individual particles, both properties that are important to understanding the current morphology and evolutionary path of the comet. Our major results are following.

6.1. Low albedo, and wide range of albedos

Borrelly has an extremely low geometric albedo, comparable to the lowest albedo objects in the Solar System such as the dark hemisphere of Iapetus (Buratti and Mosher, 1995), the darkest C-type asteroids (Tedesco et al., 1989), and the uranian rings (Ockert et al., 1987), as well as other comets (Campins et al., 1987; Veeder et al., 1987). Comets are unique among these objects in that they commonly penetrate the inner Solar System. The low albedo material that is shared by Borrelly and many objects in the outer Solar System has been loosely linked with pre-biotic material, and comets have been proposed as the transport mechanisms for bringing these precursors of life into the inner Solar System. The non-detection of water by DS1 on the surface of Borrelly (Soderblom et al., 2002) suggests a devolatized surface rich in a low-albedo lag deposit of opaque, refractory materials.

Unlike other very low albedo objects Borrelly exhibits a large range in albedo, up to a factor of three. (The exception of course is Iapetus, but its surface appears to be an admixture of two separate components; see Buratti and Mosher, 1995.) Because individual areas on the comet have different single particle phase functions, which suggests different particle sizes, shapes, or size distribution, some of the change in albedo may be due to particle size. As a whole, Borrelly is backscattering, a characteristic it shares with other planetary surfaces (e.g., Buratti, 1991; Clark et al., 1999). However, at least one area of Borrelly scatters isotropically between 52° and 76°, a characteristic not shared by any other planetary surface, but rather typical of cometary dust, including that emitted from Borrelly (Soderblom et al., 2002).

The Bond albedo of Borrelly is only 0.009, lower than any so far measured for an object in the Solar System. This low value is in part responsible for the high temperature of 300–345 K observed for Borrelly's surface during the encounter (Soderblom et al., 2002). If such low Bond albedos are typical of comets, it means that the comet's highly absorbing surface drives the heating and sublimation of volatiles. A feedback mechanism would result as the comet became active: As the surface sublimates, outgasses and darkens, its Bond albedo becomes less, making it even more absorbing.

6.2. Physical photometric parameters

In addition to differences in the single particle phase function, Borrelly exhibits differences in macroscopic roughness on its surface. The "mottled" terrain, which seems to be more extensively outgassed due to its lower albedo and what appear to be outgassed regions, is slightly smoother than the "smooth" terrain. This result suggests that the outgassing and annealing process leads to a smooth crust. Alternatively (or in addition), low-lying areas of the dormant regions could act as collection basins for cometary particles that do not leave the surface. The net result would be a smoothing of the comet's surface in these regions. Within our error bars, the global roughness of Borrelly is similar to that of other small bodies.

Whipple's original icy-conglomerate model for cometary nuclei traced out a path for the evolution of comet surface morphology (Whipple, 1950). The original surface was irregular due the comet's origin as an agglomeration of planetesimals. As the comet devolatized during successive passages into the inner Solar System, dark clumps ("globs"), which may have been the more rigid, less volatile cores of these planetesimals, develop on the surface. These comparatively resistant globs develop into spires or mounds that can break off and be carried away (Donn and Rahe, 1982) or even come off the comet in spectacular splitting events, as may have been the case with Borrelly about a week before encounter (Rayman, 2002). A quantitative model for the evolution of surface morphology (Colwell et al., 1990) suggests

that whether a comet gets "rougher" or "smoother" with time depends on the shape of the original topographic feature and the distance from the sun. In general, comets in the inner Solar System should get rougher with time. However, whether roughness is in fact increasing depends on whether the globs stay on the surface. Our results suggest that they do not. Alternatively, low-lying areas on the comet could be infilled with particles that are unable to leave the surface. Such infilling was observed in high resolution NEAR images of 433 Eros, in the "ponded deposits" that appear to embay preexisting topography (Robinson et al., 2001).

6.3. The existence of a regolith

The existence of an opposition surge on Borrelly and our preliminary result of a very fluffy surface—more fluffy than any asteroid—implies the existence of a regolith. We emphasize the preliminary nature of this result, which is based on a model-fit rather than detailed measurements of a surge (Fig. 3). In fact, the one point obtained at a very small phase angle lies below our model fit. Our result that regions of the surface exhibit particle phase functions like that of cometary dust rather than planetary surfaces offers strong evidence for the development of a regolith consisting of native dust particles that are unable to leave the comet (Whipple, 1950). This view is also supported by the lack of craters on Borrelly's surface (Soderblom et al., 2002), suggesting that meteoritic bombardment is not the controlling mechanism in the development of the regolith. Rickman et al. (1990) show that a stable dust mantle is likely on a short period comet, although a perihelion distance of 2 AU or greater enhances its development. It is important in the coming years to observe Borrelly near opposition at aphelion, during which the opposition surge can be more quantitatively measured and modeled in terms of particle size, size distribution, and compaction state. In general, this is an important measurement for comets that has not yet been done. Borrelly will have an apparition in the summer of 2005 ideally suited for measuring an opposition solar phase curve. The minimum solar phase angle will be 0.22 at new moon, with a visual magnitude of 19.1.

6.4. Relationship with asteroids and meteorites

At least 10 asteroids in comet-like orbits have albedos in the 0.019–0.038 range, suggesting they may be extinct comets (Fernandez et al., 2001). Our results also show that Borrelly has photometric properties very similar to the darkest type of asteroids, the C class (Fig. 10). The solar phase curve of Borrelly is also remarkably similar to that of 253 Mathilde, the only C-type asteroid visited by a spacecraft (Clark et al., 1999). However, if Mathilde is typical, C-type asteroids are far more uniform in albedo. One model of the comet to asteroid transition has successively larger regions of the comet converted to inert crust as outgassing progresses (Opik, 1963). This model is problematical from the DS1 data, as the outgassed regions have albedos in the 0.01 to 0.02 range, lower than the darkest asteroids (Tedesco et al., 1989). One possible modification is to have some dormant areas covered by particles that have fallen back onto the surface and rendered those regions even more inactive, an idea that is also consistent with our result that the dormant regions of the comet are less rough. These particles would tend to collect in the low-lying regions of the comet, as seems to be the case of the medium albedo ($p \sim 0.025$), uniform region adjacent to the bright spot in the widest section of the comet. This model would still lead to more albedo variegations than are seen on asteroids, although only three low-albedo asteroids have been investigated in detail for albedo variegations (253 Mathilde, and Phobos and Deimos, which are almost certainly captured asteroids). Furthermore, models suggest that inactive areas of the comet can be reactivated by explosive events caused by internal heat sources (Prialnik and Bar-Nun, 1988). Perhaps "space weathering," the phenomenon that causes S-type asteroids to darken and redden with increased exposure (Chapman, 1996) works on C-type material as well. However, Clark et al. (1999) found that it is unlikely that space weathering affected the optical properties of 253 Mathilde. The DS1 images support the idea that the active jets come from regions that are a small fraction of the comet's surface area (Sekanina, 1991). However, global sublimation of volatiles, driven by Borrelly's very low Bond albedo, may play an important role in the outgassing of comets and the evolution of their surfaces (Weissman and Kieffer, 1981).

The association of numerous Earth-crossing comets with meteor showers has raised the possibility that comets night be the source of at least some of the carbonaceous chondrites. Proving an association would be important, since these meteorites could then be considered a sample of a comet's nucleus. Comets were once proposed to be the source of meteorites, due to the difficulty of moving asteroids from the main belt to the inner Solar System (Opik, 1966), but recent inventories of hundreds of NEAs obviates that difficulty. The exact connections between comets, asteroids, and meteorites are elusive and a number of details concerning composition, spectra, structure, and albedo, do not work out. Our results only add to the number of these details. First, the average normal reflectance of Borrelly is at the very lowest end of the measured range of 0.03–0.11 for carbonaceous chondrites (Gaffey, 1976; Johnson and Fanale, 1973). When one considers that the lowest albedos on Borrelly are in the 0.01 range, the discrepancy becomes even more problematical. A Bond albedo of 0.06 in the visible region has been measured for one carbonaceous chondrite, Murchison (French, 1980), which is far higher than Borrelly's. Finally, the phase function of Murchison is not nearly as steep as that of Borrelly (French, 1980). If meteorites represent the most refractory, lowest albedo part of the incoming meteoroid, devoid of native volatiles that sublimate in the terrestrial atmosphere, it is difficult to reconcile our results with comets being the source of the carbonaceous chondrites.

Acknowledgments

This work was performed at the Jet Propulsion Laboratory, California Institute of Technology, under contract to the National Aeronautics and Space Administration. We thank Drs. Paul Weissman and Martha Hanner for their detailed comments on this paper, and Drs. G. Tancredi and I. Toth for their reviews. Dr. Tancredi provided additional data for Fig. 3. This work was supported in part by the NASA Planetary Geology and Planetary Astronomy Programs.

References

A'Hearn, M.F., Millis, R.L., Schleicher, D.G., Osip, D.J., Birch, P.V., 1995. The ensemble properties of comets: results from narrowband photometry of 85 comets, 1976–1992. Icarus 118, 223–270.

Belton, M., 1991. Characterization of the rotation of cometary nuclei. In: Newburn, R.L., Neugebauer, M., Rahe, J. (Eds.), Comets in the Post-Halley Era, Vol. 1. Kluwer Academic, Dordrecht, pp. 691–721.

Britt, D., Boice, D.C., Buratti, B.J., Hicks, M.D., Nelson, R.M., Oberst, J., Sandel, B.R., Soderblom, L.A., Stern, S.A., Thomas, N., 2002. The geology of Comet 19P/Borrelly. In: Proc. Lunar Planet. Sci. Conf. 33rd. Abstract 1686.

Buratti, B.J., 1985. Voyager disk resolved photometry of the saturnian satellites. Icarus 59, 392–405.

Buratti, B.J., 1991. Ganymede and Callisto: surface textural dichotomies and photometric analysis. Icarus 92, 312–323.

Buratti, B.J., Veverka, J., 1983. Voyager photometry of Europa. Icarus 55, 93–110.

Buratti, B.J., Veverka, J., 1985. Photometry of rough planetary surfaces: the role of multiple scattering. Icarus 64, 320–328.

Buratti, B.J., Mosher, J.A., 1995. The dark side of Iapetus: additional evidence for an exogenous origin. Icarus 115, 219–227.

Campbell, D.B., Harmon, J.K., Shapiro, I.I., 1989. Radar observations of Comet Halley. Astrophys. J. 338, 1094–1105.

Campins, H., A'Hearn, M.F., McFadden, L.A., 1987. The bare nucleus of Comet Neujmin 1. Astrophys. J. 316, 847–857.

Chandrasekhar, S., 1960. Radiative Transfer. Dover, New York.

Chapman, C.R., 1996. S-type asteroids, ordinary chondrites, and space weathering: the evidence from Galileo's fly-bys of Gaspra and Ida. Meteoritics 31, 699–725.

Clark, B.E., Veverka, J., Helfenstein, P., Thomas, P.C., Bell III, J.F., Harch, A., Robinson, M.S., Murchie, S.L., McFadden, L.A., Chapman, C.R., 1999. NEAR photometry of Asteroid 253 Mathilde. Icarus 140, 53–65.

Colwell, J.E., Jakosky, B.M., Sandor, B.J., Alan Stern, S., 1990. Evolution of topography on comets. Icarus 85, 205–215.

Delahodde, C.E., Meech, K.J., Hainaut, O., Dotto, E., 2001. Detailed phase function of Comet 28P/Neujmin 1. Astron. Astrophys. 376, 672–685.

De Pater, I., Lissauer, J., 2001. Planetary Sciences. Cambridge Univ. Press, Cambridge, UK.

Donn, B., Rahe, J., 1982. Structure and origin of cometary nuclei. In: Wilkening, L. (Ed.), Comets. Univ. of Arizona Press, Tucson.

Fernandez, Y.R., Jewitt, D.C., Sheppard, S.S., 2001. Low albedos among extinct comet candidates. Astrophys. J. 553, L97–L200.

Fink, U., Hicks, M.D., Fevig, R.A., 1995. Production rates for the Stardust mission target: 81P/Wild 2. Icarus 141, 331–340.

French, L., 1980. Photometric properties of carbonaceous chondrites and related materials. PhD dissertation. Cornell University, Ithaca, NY.

Gaffey, M.J., 1976. Spectral reflectance characteristics of the meteorite classes. J. Geophys. Res. 81, 905–920.

Hapke, B., 1984. Bidirectional reflectance spectroscopy. 3. Correction for macroscopic roughness. Icarus 59, 41–59.

Hapke, B., 1986. Bidirectional reflectance spectroscopy. 4. The extinction coefficient and the opposition effect. Icarus 67, 264–280.

Hapke, B., 1990. Coherent backscatter and the radar characteristics of outer planet satellites. Icarus 88, 407–417.

Harmon, J.K., Campbell, D.B., Hine, A.A., Shapiro, I.I., Marsden, B.G., 1989. Radar observations of Comet IRAS–Araki–Alcock 1983d. Astrophys. J. 338, 1071–1093.

Helfenstein, P., Veverka, J., 1989. Physical characterization of asteroid surfaces from photometric analysis. In: Binzel, R., Gehrels, T., Matthews, M.S. (Eds.), Asteroids II. Univ. of Arizona Press, Tucson, pp. 557–593.

Helfenstein, P., Veverka, J., Thomas, P.C., 1988. Uranus satellites: Hapke parameters from Voyager disk integrated photometry. Icarus 74, 231.

Helfenstein, P., 23 colleagues, 1994. Galileo photometry of Asteroid 951 Gaspra. Icarus 107, 37–60.

Helfenstein, P., 10 colleagues, 1996. Galileo photometry of Asteroid 243 Ida. Icarus 120, 48–65.

Henyey, L.G., Greenstein, J., 1941. Diffuse radiation in the Galaxy. Astrophys. J. 93, 70–83.

Hicks, M., 1997. A spectrophotometric survey of comets and Earth-approaching asteroids. PhD dissertation. University of Arizona, Tucson.

Hillier, J.K., Buratti, B.J., Hill, K., 1999. Multispectral photometry of the Moon and absolute calibration of the Clementine UV/Vis camera. Icarus 141, 205–2225.

Horak, H.G., 1950. Diffuse reflection by planetary atmospheres. Astrophys. J. 112, 445–463.

Hughes, D.W., 1985. The size, mass, mass loss and age of Halley's comet. Mon. Not. R. Astron. Soc. 211, 103–109.

Jewitt, D., 1991. Cometary photometry. In: Newburn, R.L., Neugebauer, M., Rahe, J. (Eds.), Comets in the Post-Halley Era, Vol. 1. Kluwer Academic, Dordrecht, pp. 19–65.

Johnson, T.V., Fanale, F.P., 1973. Optical properties of carbonaceous chondrites and their relationship to asteroids. J. Geophys. Res. 78, 8507–8518.

Keller, U., 1990. The nucleus. In: Huebner, W.F. (Ed.), Physics and Chemistry of Comets. Springer-Verlag, Berlin.

Lamy, P.L., Toth, I., Weaver, H.A., 1998. Hubble Space Telescope observations of the nucleus and inner coma of Comet 19P/1904 Y2 (Borrelly). Astron. Astrophys. 337, 945–954.

Lamy, P.L., Toth, I., Fernandez, Y.R., Weaver, H.A., 2003. The sizes, shapes, albedos, and colors of cometary nuclei. In: Comets II. Univ. of Arizona Press, Tucson. In press.

Lane, A.P., Irvine, W.H., 1973. Monochromatic phase curve and albedos for the lunar disk. Astron. J. 78, 267–277.

Licandro, J., Tancredi, G., Lindgren, M., Rickman, H., Hutton, R.G., 2000. CCD photometry of cometary nuclei. I. Observations from 1990–1995. Icarus 147, 161–179.

Lowry, S.C., Fitzsimmons, A., 2001. CCD photometry of distant comets II. Astron. Astrophys. 365, 204–213.

Luu, J., 1993. Spectral diversity among the nuclei of comets. Icarus 104, 138–148.

Meech, K., 1991. Physical aging in comets. In: Newburn, R.L., Neugebauer, M., Rahe, J. (Eds.), Comets in the Post-Halley Era, Vol. 1. Kluwer Academic, Dordrecht, pp. 629–669.

Noland, M., 1975. Photometriatellites of Saturn. PhD dissertation. Cornell University, Ithaca, NY.

Ockert, M.E., Cuzzi, J.N., Porco, C.C., Johnson, T.V., 1987. Uranian ring photometry: results from Voyager 2. J. Geophys. Res. 92, 14969–14978.

Opik, E., 1963. Survival of cometary nuclei and the asteroids. Adv. Astron. Astrophys. 2, 219–262.

Opik, E., 1966. The stray bodies in the Solar System II. The cometary origin of meteorites. Adv. Astron. Astrophys. 4, 302–336.

Prialnik, D., Bar-Nun, A., 1988. The formation of a permanent dust mantle and its effect on cometary activity. Icarus 74, 272–283.

Rayman, M., 2002. The successful conclusion of the Deep Space 1 Mission: important results without a flashy title. Paper presented at the 53rd Annual International Astronautical Congress/World Space Congress, October 10–19, 2002, Houston, TX.

Rauer, H., Hahn, G., Harris, A., Helbert, J., Mottola, S., Oberst, J., 1999. Nuclear parameters of Comet P/Borrelly. Bull. Am. Astron. Soc. 31, 1131.

Rickman, H., Fernandez, J.A., Gustafson, B.A.S., 1990. Formation of stable dust mantles on short-period comet nuclei. Astron. Astrophys. 234, 524–535.

Robinson, M.S., Thomas, P.C., Veverka, J., Murchie, S., Carcich, B., 2001. The nature of ponded deposits on Eros. Nature 423, 396–400.

Sagdeev, R.Z., Avanesov, G.A., Ziman, Y.L., Moroz, V.I., Tarnopolsky, V.I., Zhukov, B.S., Shamis, V.A., Smith, B., Toth, I., 1986. TV experiment of the Vega mission: photometry of the nucleus and the inner coma. In: Battrick, B., Rolfe, E.J., Reinhard, R. (Eds.), 20th ESLAB Symposium on the Exploration of Halley's Comet II. In: ESA SP, Vol. 250, pp. 317–326.

Sekanina, Z., 1991. Cometary activity, discrete outgassing areas, and dust-jet formation. In: Newburn, R.L., Neugebauer, M., Rahe, J. (Eds.), Comets in the Post-Halley Era, Vol. 1. Kluwer Academic, Dordrecht, pp. 769–823.

Simonelli, D.P., Wisz, M., Switala, A., Adinolfi, D., Veverka, J., Thomas, P.C., Helfenstein, P., 1998. Photometric properties of Phobos surface materials from Viking images. Icarus 131, 52–77.

Soderblom, L.A., 21 colleagues, 2002. Observations of Comet 19P/Borrelly by the miniature integrated camera and spectrometer aboard Deep Space 1. Science 296, 1087–1091.

Squyres, S., Buratti, B.J., Veverka, J., Sagan, C., 1984. Voyager photometry of Iapetus. Icarus 59, 426–435.

Tedesco, E., Williams, J.G., Matson, D.L., Veeder, G.L., Gradie, J.C., Lebofsky, L.A., 1989. A three-parameter asteroid taxonomy. Astron. J. 97, 580.

Thomas, P.C., Adinolfi, D., Helfenstein, P., Simmelli, D., Veverka, J., 1996. The surface of Deimos: contribution of materials and processes to its unique appearance. Icarus 123, 536–556.

Tokunaga, A.T., Hanner, M.S., Golish, W.F., Griep, D.M., Kaminski, C.D., 1992. Infrared monitoring of Comet P/Tempel 2. Astron. J. 104, 1611–1617.

Veeder, G., Hanner, M.S., Tholen, D.J., 1987. The nucleus of Comet P/Arend–Rigaux. Astron. J. 94, 169–173.

Veverka, J., 1970. Photometric and polarimetric studies of minor planets and satellites. PhD Thesis. Harvard University, Cambridge, MA.

Veverka, J., Goguen, J., Yang, S., Elliot, J.L., 1978. Scattering of light from particulate surfaces. Icarus 34, 406–414.

Veverka, J., 15 colleagues, 1997. NEAR's flyby of Mathilde: the first look at a C-type asteroid. Science 278, 2109–2114.

Weissman, P.W., Kieffer, W., 1981. Thermal modeling of cometary nuclei. Icarus 47, 302–311.

Weissman, P.W., Doressoundiram, A., Hicks, M., Chamberlin, A., Sykes, M., Larson, S., Hergenrother, C., 1999. CCD photometry of comet and asteroid targets of spacecraft missions. Bull. Am. Astron. Soc. 31, 1131.

Weissman, P.W., Bottke, W.F., Levison, H.F., 2003. Evolution of comets into asteroids. In: Bottke, W.F., Celllino, A., Paolicchi, P., Binzel, R. (Eds.), Asteroids III. Univ. of Arizona Press, Tucson, pp. 669–686.

Whipple, F., 1950. A comet model I. The acceleration of Comet Encke. Astrophys. J. 111, 375–394.